HHS Public Access

Author manuscript

IEEE Trans Med Imaging. Author manuscript; available in PMC 2016 March 01.

Published in final edited form as:

IEEE Trans Med Imaging. 2015 March ; 34(3): 740–747. doi:10.1109/TMI.2014.2358561.

Spectral CT Using Multiple Balanced K-Edge Filters

Yothin Rakvongthai[*],
Center for Advanced Medical Imaging Sciences, Massachusetts General Hospital, Boston, MA 02114, USA, and also with the Department of Radiology, Harvard Medical School, Boston, MA 02115, USA

William Worstell[*],
PhotoDiagnostic Systems Inc., Boxboro, MA 01719, USA.

Georges El Fakhri [Senior Member, IEEE],
Center for Advanced Medical Imaging Sciences, Massachusetts General Hospital, Boston, MA 02114, USA.

Department of Radiology, Harvard Medical School, Boston, MA 02115, USA.

Junguo Bian [Member, IEEE],
Center for Advanced Medical Imaging Sciences, Massachusetts General Hospital, Boston, MA 02114, USA.

Department of Radiology, Harvard Medical School, Boston, MA 02115, USA.

Auranuch Lorsakul [Student Member, IEEE], and
Center for Advanced Medical Imaging Sciences, Massachusetts General Hospital, Boston, MA 02114, USA.

Department of Biomedical Engineering, Columbia University, New York, NY 10027, USA.

Jinsong Ouyang[**] **[Senior Member, IEEE]**
Center for Advanced Medical Imaging Sciences, Massachusetts General Hospital, Boston, MA 02114, USA.

Department of Radiology, Harvard Medical School, Boston, MA 02115, USA.

Abstract

Our goal is to validate a spectral CT system design that uses a conventional X-ray source with multiple balanced K-edge filters. By performing a simultaneously synthetic reconstruction in multiple energy bins, we obtained a good agreement between measurements and model expectations for a reasonably complex phantom. We performed simulation and data acquisition on a phantom containing multiple rods of different materials using a NeuroLogica CT scanner. Five balanced K-edge filters including Molybdenum, Cerium, Dysprosium, Erbium, and Tungsten were

[**]Corresponding author: Jinsong Ouyang (ouyang.jinsong@mgh.harvard.edu).
Yothin Rakvongthai is now with the Department of Radiology, Faculty of Medicine, Chulalongkorn University, Bangkok, Thailand.
[*]Co-first authors

used separately proximal to the X-ray tube. For each sinogram bin, measured filtered vector can be defined as a product of a transmission matrix, which is determined by the filters and is independent of the imaging object, and energy-binned intensity vector. The energy-binned sinograms were then obtained by inverting the transmission matrix followed by a multiplication of the filter measurement vector. For each energy bin defined by two consecutive K-edges, a synthesized energy-binned attenuation image was obtained using filtered back-projection reconstruction. The reconstructed attenuation coefficients for each rod obtained from the experiment was in good agreement with the corresponding simulated results. Furthermore, the reconstructed attenuation coefficients for a given energy bin, agreed with National Institute of Standards and Technology reference values when beam hardening within the energy bin is small. The proposed cost-effective system design using multiple balanced K-edge filters can be used to perform spectral CT imaging at clinically relevant flux rates using conventional detectors and integrating electronics.

Index Terms

Spectral CT; Rainbow-CT; K-edge filters; Ross spectrometer; transmission matrix

I. Introduction

Conventional CT delivers sub-optimal images at greater than necessary dose to the patient because it combines poly-spectral X-ray flux indiscriminately. Conventional CT cannot make use of the X-ray energy dependence of attenuation coefficients to distinguish material types. As a result, contrast is insufficient for some diagnostic purposes and patient X-ray dose is not used in a maximally efficient manner [1].

Although recently-commercialized Dual-energy CT (DECT) systems improve quantitative accuracy and reduce metal artifacts as compared to conventional CT, further improvement in each of these areas is still needed [2, 3]. Improvement in each of these areas should not decrease performance in any of the other areas, and preferably should not increase system costs. In practice, phantom measurements show that DECT effective atomic number measurements are inaccurate at low energies for dense tissues and vary with surrounding tissue thicknesses [2, 4]. DECT can, in principle, correct for beam hardening by low-Z materials, but has limited quantitative accuracy in practice. DECT is particularly limited when either metal or materials with one or more K-edges (e.g. one or more contrast media) are in the field of view (FOV) [5].

Spectral CT (SCT) separates CT attenuation data into more than two X-ray energy-determined spectral bins and thereby allows more materials to be distinguished in a single acquisition [6]. In addition, SCT can make use of absorption edges (“K-edges”) in the energy range of interest, which are characteristic of higher-Z materials that can be used as advanced imaging contrast agents [7, 8]. Unfortunately, current SCT detectors are expensive, and are quantitatively inaccurate when operating at the X-ray fluxes needed for clinical CT [9]. Current photon-counting SCT detectors have pronounced spectral distortions due to pileup and charge sharing effects [10], and are difficult to calibrate [11]. Free-

electron and synchrotron sources for mono-energetic X-rays have been proposed, but are expensive and impractical [12]. A more practical source of quasi-mono-energetic X-rays uses heavy K-edge filtering of characteristic X-rays, as has been applied to mammography and breast CT, but this yields low beam flux, is restricted to particular X-ray filters and energies, and is not amenable to multiple energy windows [13].

We make use of thin K-edge filters of precisely known composition, in particular thin foils of rare earth elements, to accomplish this controlled and source X-ray flux rate-independent spectral modulation. In this work, we propose a "Rainbow-CT" design that combines a CT scanner with a Ross spectrometer. We obtain energy-binned sinograms via the inverse of a transmission matrix that connects the measured filtered intensity vector and an energy-binned intensity vector.

Ross filter pairs, sometimes called balanced filter pairs, consist of a pair of filters with adjacent or nearly adjacent atomic numbers whose thicknesses are such that the transmitted spectra through the two filters are nearly identical except in the energy band between their respective K-edges [14]. By subtracting the X-ray signal seen through a filter with the lower K-edge from that with the higher K-edge in a Ross pair, one obtains the equivalent of a nearly quasi-mono-energetic X-ray beam spectrum with energies bounded by the two K-edge energies. Mono-energetic beams avoid the beam hardening of poly-energetic X-ray beams, which is an important source of artifacts and quantitative inaccuracy in CT [15]. Ross filter pairs are used in X-ray diagnostic instrumentation for tokamaks and high-power laser facilities, including as filter pair sets where they can be used to form a Ross X-ray spectrometer [16]. Saito introduced Ross filters into CT, using a Ross pair bracketing a tungsten characteristic X-ray line to generate a synthetic quasi-mono-energetic X-ray beam [17].

Rainbow-CT avoids the cost, complexity, rate-limitations and spectral/calibration distortions of photon-counting SCT sensors, while preserving their advantages for K-edge and multiple contrast agent imaging. This potentially enables operation at a single adjustable kVp. Furthermore, a significant potential benefit of Rainbow-CT is improved quantitative accuracy. Rainbow-CT is fundamentally stable and robust in its spectral measurement method because it defines its spectral boundaries by the intrinsic material properties (K-edge energies) of its modulating filters, which have unvarying thickness, precisely known spectral properties, and require only the assumption of a spectrally unvarying source upstream of the filters. Thus Rainbow-CT provides the potential basis for a cost-effective and practical implementation of SCT using conventional CT detectors and electronics.

The novelties of this work are: 1) We proposed a Rainbow-CT technique, which is a spectral CT technique using Ross spectrometer (multiple balanced K-edge filters) with conventional CT scanner. 2) To compensate for non-perfectly balanced filters, we proposed a transmission matrix based method to obtain energy-resolved sinograms from measured CT intensities using the filters. We validated our approach and studied its systematic errors in both simulation and experimental phantom studies.

II. Methods

A. Rainbow-CT Technique

The proposed Rainbow-CT method uses a Ross spectrometer, which is a set of balanced K-edge filters. The thicknesses of these filters are chosen so that the transmitted X-ray energy spectra are almost identical except in the energy band between their respective K-edges. For a given sinogram bin, subtracting the intensity acquired using one filter from the intensity acquired using another filter with higher K-edge yields a measure proportional to the energy-weighted flux intensity within the energy bin bounded by the K-edges of the two filters. When a standard CT operates at 80 kVp, Fig. 1(A) shows the energy spectra seen through five different filters [Molybdenum (Mo), Cerium (Ce), Dysprosium (Dy), Erbium (Er), and Tungsten (W)], while the 80 kVp poly-energetic beam is energy resolved via the Ross spectrometer principle in Fig. 1(B). Fig. 1(C) displays the ratio of energy-dependent attenuation coefficients of two consecutive filters. If the filters' thicknesses are precisely matched, the sinogram collected using one member of each Ross filter pair within the spectrometer may be subtracted from that of its Ross-pair partner, thereby yielding an energy-binned sinogram. In principle, Ross filters are to be carefully matched in thickness, but below we propose and validate a method for compensating for small differences from ideal thicknesses for any set of filters. Performing this operation both with an object in the FOV and without (blank scan), we can obtain a pair of energy-binned sinograms. By taking the logarithm of the ratio of these two sinograms, we obtain an energy-binned attenuation sinogram, i.e. line integrals of attenuation coefficients (μ) specific to the relatively narrow energy band of interest.

While it is reasonable to fix the low-energy ends of the Rainbow-CT to cover the range of energies expected to be significantly transmitted through a typical object (i.e. differently for pre-clinical or extremities imaging than for abdominal clinical imaging), an object in an energy window where the flux is heavily attenuated will just be reconstructed as opaque in that energy range. For the high-energy end of the Rainbow-CT, one needs to go only as high as the highest anticipated K-edge contrast material, which could be set either just above Gadolinium or just above Gold [18]. In this work, we used thin foils of Mo, Ce, Dy, Er, and W with nominal thicknesses of 8, 6, 3, 3, and 1 mil (1 mil = 25.4 μm) respectively, but other choices of materials with correlated thicknesses are possible. These thicknesses were chosen to minimize tube-loading while still achieving significant contrast between filter pairs. In principle, Ross filters are to be carefully matched in thickness, but one may either modify their effective thickness by "shimming" with lower-Z materials [19] or invert the transmission matrix for any set of filters of known thickness as discussed below. For a set of well-matched filters, the sum of squared difference of the two energy-dependent attenuation factors outside the pass-band for any of the two filters is minimized. However, the filter thickness values as ordered from the filter manufacture, called nominal thickness values, are usually different from the well-matched values. For a set of filters with nominal thickness values, we call it nearly-matched filter set throughout this paper.

An important test of the accuracy with which we can model the proposed Rainbow-CT technique, which will be fundamental to the development of accurate model-based image

reconstruction of this system, is quasi-mono-energetic imaging with the linear analytic filtered backprojection (FBP) image reconstruction algorithm. In the method described below, measurement modeling allows us to obtain intensities in energy bins bracketed by filters' K-edge energies via the inverse of a transmission matrix. The measurement modeling for the Rainbow-CT can be described as follows.

For the *i*-th detector (sinogram) bin, the measured intensity, $y_{i,l}^{F}$ using the *l*-th filter can be modeled as:

$$y_{i,l}^{F}=\sum_{k=1}^{N_E} b_{i,l}^{k} y_{i,k} \quad (1)$$

where N_E is the number of energy bins, $y_{i,k}$ is the intensity that would be detected in the *i*-th detector bin and the *k*-th energy bin ($k = 1,2, \ldots, N_E$) as if no filter is used, and $b_{i,l}^{k}$ is computed using:

$$b_{i,l}^{k}=\frac{\int_{E_{k-1}}^{E_k} \exp(-\mu_l(E) t_{i,l}/\cos\theta_i) dE}{E_k - E_{k-1}} \quad (2)$$

where $\mu_l(E)$ is the attenuation coefficient for the *l*-th filter at energy *E*, $(E_{k-1}, E_k]$ is the energy range of the *k*-th energy bin, $t_{i,l}$ is the *l*-th filter thickness at the point where the line connecting the X-ray beam spot and the *i*-th detector bin intercepts the filter, and θ_i is the angle between the normal of the filter surface and the line connecting the X-ray beam spot and the *i*th detector bin In the matrix-vector format, the model can be described by

$$\mathbf{Y}_i^{F}=\mathbf{B}_i \mathbf{Y}_i \quad (3)$$

Where $\mathbf{Y}_i^{F}=[y_{i,1}^{F}, \ldots, y_{i,N_F}^{F}]^T$, $\mathbf{Y}_i = [y_{i,1}, \ldots, y_{i,N_E}]^T$, and $\mathbf{B}_i = \left\{b_{i,l}^{k}\right\}$. Therefore, we can determine the energy-binned intensity for the *i*-th detector bin by solving for $\mathbf{Y}_i$ in Eq. (3). Based on the K-edge energies of the filters, K_i, we define energy bins: $(0, K_1]$, $(K_1, K_2]$, …, $(K_{NF}, E_{kVp}]$, i.e. $E_0 = 0$, $E_k = K_k$ for $k = 1, .., N_F$ (N_F is the number of K-edge filters), and $E_{N_E} = E_{kVp}$, which is the X-ray maximum energy corresponding to the tube voltage. By doing so, $\mathbf{B}_i$ has a dimension of $N_F \times N_E$, where $N_E = N_F + 1$. For Eq. (3), we chose the least-square solution that can be computed by multiplying $\mathbf{Y}_i^{F}$ with the pseudoinverse of $\mathbf{B}_i$ using:

$$\hat{\mathbf{Y}}_i=\mathbf{B}_i^T(\mathbf{B}_i\mathbf{B}_i^T)^{-1}\mathbf{Y}_i^{F} \quad (4)$$

For matched filters, the energy spectrum for either $(0, K_1]$ or $(K_{NF}, E_{kVp}]$ is almost the same for all the filters. This implies that it is impossible to have non-zero spectrum in $(0, K_1]$ and zero spectrum in the other (and vice versa) regardless how filter spectra are linearly combined because the energy spectra in these two energy bins change in the same way. Therefore, we exclude both $(0, K_1]$ and $(K_{NF}, E_{kVp}]$. Reconstructing energy-binned intensity estimates obtained by Eq. (4) yields energy-binned CT images for the $N_F - 1$ middle energy bins. For a well-matched balanced filter set, the sub-matrix corresponding to the middle bins

of this pseudoinverse matrix is exactly bi-diagonal, while for a slightly mismatched filters of known thickness it is nearly so.

B. CT Simulation

We performed phantom simulation using a CT system with the same geometry as the one used for the phantom experiment described in Sec. II-C. Five filters including Mo, Ce, Dy, Er, and W, were used in the simulation, i.e. $N_F = 5$, and $N_E = 6$. The energy bins defined by the K-edges of these filters are: 20.0–40.4, 40.4–53.8, 53.8–57.5, and 57.5–69.5 keV. The simulation phantom had a 20-cm polyvinyl chloride (PVC) background, a 5-cm water rod in the center and six embedded 2.8-cm Gammex rods (Gammex Inc., Middleton, Wisconsin) including Adipose, CB2-30, Cortical Bone, Liver, Solid Water, and Lung-300. The material properties of these rods are given by the vendor as well as in [20]. The X-ray spectrum was simulated at 80 kVp using Spektr [21] software. Projection data were simulated from a regular arc detector array via ray tracing, with energy-weighted integrals over 1 keV spectral steps. There was no noise added to the simulated projection data. We performed the simulation using both well- and nearly-matched thickness for each filter.

C. CT Experiment

We acquired phantom data on a CereTom scanner (Neurologica Corporation, Danvers, Massachusetts) shown in Fig. 2(A). The X-ray source has 1×1 mm^2 beam spot. The scanner has 17 detector modules mounted on a rotatable gantry, where the last module is the reference module and was not used in the reconstruction. Each module has a 24×8 pixel array with 1.08×2.27 mm^2 pixel size (transverse×axial). The phantom is a PVC plate with a 5-cm cylindrical water inserted at the center and six Gammex 2.8-cm rods inserted on the side [See Fig. 2(B)]. The rods included Adipose, CB2-30, Cortical Bone, Liver, Titanium-embedded Solid Water, and Lung-300 rods. We used a set of balanced K-edge filters including Mo, Ce, Dy, Er, and W. For each filter, we acquired 12-second and 2-second phantom and blank data, respectively. We also acquired data without using any filter for both phantom and blank scans. All the data were acquired at 80 kVp/7 mA and 30 rpm with 1440 views/rotation.

For a given filter, the interception length in the filter by the ray from the X-ray beam spot to each detector bin must be known in order to compute the transmission matrix. For the simulation study, the thickness of each filter used to compute the transmission matrix is the same as the input to the simulation. For the experimental study, the interception thickness for each filter was calculated using two blank acquisitions: one with and the other without using the filter. Specifically, we have:

$$log\left(\frac{I_i}{I_{i,l}^F}\right) = log\left(\frac{\int ES(E)dE}{\int ES(E)e^{-\mu_l(E)t_{i,l}/\cos(\theta_i)}dE}\right) \quad (5)$$

where I_i and $I_{i,l}^F$ are the measured blank-scan intensities without and with the l-th filter. We solved this equation to find $t_{i,l}$ using Newton-Raphson iterative algorithm. The initial estimate used for the iterative algorithm was the measured filter thickness, which was

determined by measuring filter area with micrometers and weighing the filter with a milligram scale.

D. Image Reconstruction and Quantitative Analysis

Both the simulated and experimental data in each energy bin were reconstructed using a 2D FBP algorithm (MATLAB's ifanbeam function) with 0.5×0.5×0.5 mm^3 voxel size and Hamming filter (0.8-cutoff). For the experimental data, we summed over axially adjacent detector rows and removed the metal artifacts caused by titanium using interpolation within the titanium's mask in the log-attenuation sinograms prior to the reconstruction [22], [23].

After the reconstruction, we defined a region of interest (ROI) in Adipose, CB2-30, Cortical Bone, Liver, Lung-300, and water and computed the mean μ within the ROI for each energy bin. We compared the relative error of the mean μ for both the simulation and experiment using the weighted average National Institute of Standards and Technology (NIST) μ [24] as the reference. For both the simulation and experiment, the poly-energetic images were also reconstructed using the scans in the absence of any K-edge filter. One of the inserts used in the experiment was a titanium-embedded solid water rod. The corresponding rod used in the simulation was a pure solid water rod. In order to make a fair comparison between the simulation and experiment, we did not include results for the solid water insert in this study because the interpolation used to remove the titanium contribution may introduce systematic bias.

III. Results

Fig. 3 shows the measured thicknesses of all five filters for all the detector bins for the CT experiment. The thickness non-uniformity, which is defined as the ratio between standard deviation and mean across all the detector bins, is 1.4%, 0.9%, 1.6%, 1.4%, and 2.5% for Mo, Ce, Dy, Er, and W, respectively. Insertion, removal, and re-insertion of the filters into the holder gave repeatability variations significantly smaller than this thickness variation.

For both the simulation and experiment, Fig. 4 displays the transmission and its pseudoinverse matrices for one of detector bins in the middle. Note that the pseudoinverse shows a bi-diagonal pattern.

The energy-binned sinograms and reconstructed energy-binned μ images of the simulated phantom in four energy bins (20.0–40.4, 40.4–53.8, 53.8–57.5, and 57.5–69.5 keV) are displayed in Fig. 5 for both the simulation (nominal thicknesses) and experimental studies. As expected, more beam-hardening artifacts in the form of cupping artifacts were found at lower energy bins for both studies. The cupping artifacts also seemed to be more pronounced for the simulation than for the experiment. This is likely caused by the difference between the simulated and actual source spectra given the fact that both the width and $d\mu/dE$ for the first energy bin are high as compared to other energy bins. The proposed Rainbow-CT technique yielded energy-binned μ images of the phantom. As compared to the poly-energetic image, cupping artifacts were reduced in the highest three energy bins. While the simulation images are free of ring artifacts, ring artifacts are noticeable in the experimental images for the lowest energy bin. For the experimental results, the streak

artifacts emanating from Titanium-embedded Solid Water rod resulting from the imperfect metal artifact removal was also present.

Fig. 6 shows the ROI-averaged μ values computed for all the energy bins. Good agreement between the simulation and experiment was found except CB2-30 and Cortical Bone rods for the lowest energy bin. There are no statistical errors associated with the simulation results. The experimental statistical uncertainties are very low (less than 0.42% and 0.28% for all the four energy bins and poly-energetic spectrum, respectively) because the data acquisition was long. The difference between the measured $\bar{\mu}$ and its corresponding weighted average NIST μ value for each material was tabulated in Table I. For the simulation study, the results using well-matched thicknesses were also consistent with those using nominal thicknesses.

IV. Discussions

Our main goal of the proposed study was to validate the feasibility, and to estimate the amenability to accurate modeling, of a spectral CT system design using a conventional X-ray source with a Ross spectrometer. We performed the study through the method of simultaneously synthetic reconstruction in multiple energy bins. The proposed method to use Ross spectrometer incorporating a set of nearly-matched balanced K-edge filters whose thickness values are such that the transmitted spectra through any two filters are nearly identical except in the energy band between their respective K-edges. In our framework, modeling the measurements allowed us to obtain energy-binned sinograms via a transmission matrix. The energy-binned sinograms were then reconstructed to obtain energy-binned μ images. It should be noted that the same filter thicknesses can be used for different kVp values since the spectrum variation would be accounted for in the transmission matrix.

In the simulation study, differences between measured $\bar{\mu}$ values and the known truth for the test materials largely resulted from beam hardening effects within each energy bin. The error was larger in the lowest energy bin because of wide energy-bin width and relatively high variation of μ within this bin. The simulation results for the case of well- and nearly-matched filters were consistent, which suggests robustness of the proposed approach with respect to non-ideal case in terms of filters' thicknesses.

The ROI-averaged μ values agree reasonable well between the simulation and experiment except the first energy bin for the CB2-30 and Cortical Bone rods and the second and third energy bins for the Lung-300 rod. The disagreement between the simulation and experiment may result from a few factors. First, there were still streak artifacts emanating from the Titanium-embedded Solid Water rod in energy-binned μ images due to non-perfect titanium removal. Second, scatters might also contribute to the error since our proposed model assumes perfect anti-scatter grid performance. Third, the quantitative accuracy of the experimental results was degraded by the systematic errors in the thickness measurement. Fourth, it is also the case that we have less confidence in the accuracy with which Spektr models our X-ray source spectrum in the lowest energy bins, where this spectrum is most sensitive to details of source pre-filtering. Fifth, the material reference values for all the rods

have errors. Nevertheless, particular in the higher energy bins, we obtained quite close agreement between measured and modeled μ values for most of the materials and energy bins, which holds out the prospect of potentially including correction for such effects within the context of planned model-based iterative reconstruction methods which are beyond the scope of this work.

For the proposed Rainbow-CT design, filter switching can be implemented in a few different ways. For example, filter switching can be made at the end of each detector rotation. This increases imaging time and tube loading by a factor of N_F as compared to conventional CT. Moreover, it becomes more sensitive to patient motion and change of CT contrast. Another approach is to use a rotation filter wheel in front the X-ray tube so that filter change can be made anytime during the detector rotation [25]. If filter switching can be made fast enough and properly controlled so that angular views for each filter is relatively evenly spaced, number of detector rotations required for each slice acquisition can be significantly reduced. As a result, tube loading and susceptibility to patient motion artifacts and contrast change can be minimized.

Rainbow-CT is expected less efficient to acquire energy-resolved images than photon-counting SCT because a large fraction of X-ray dose is allocated to the poly-energetic images [See Fig. 1(A) and Fig. 5]. We believe, however, the resulting poly-energetic images obtained by Rainbow-CT should be used together with all the energy-resolved images for a given clinical task.

As compared to conventional CT, Rainbow-CT requires higher tube current to achieve the same image quality for the same imaging time because X-ray attenuation within filters. However, in clinical practice, tube current is adjusted based on patient size. The maximum tube current is not used for most cases. Generally speaking, Rainbow-CT requires higher tube current or more imaging time if maximum tube current is reached.

Our future work with this system is expected to follow several tracks. First, we will continue to refine our characterization of the system and in particular our X-ray source spectrum at lower energies, to obtain better correspondence between modeled expectations and measurements. Second, we will compare the performance of our spectral CT approach to DECT and photon-counting SCT in terms of contrast-to-noise ratio per unit dose and material decomposition. Third, we will experiment with imaging objects with significant K-edges within the energy range of interest (i.e. iodinated and Gd-loaded contrast agents). Fourth, we will continue to develop methods to decrease metal artifact, including methods which take advantage of spectrally-resolved information along lines of response intersecting the metal. Finally, we will incorporate our modeled system response results within a model-based iterative image reconstruction algorithm framework, which should also help to mitigate metal artifacts.

V. Conclusion

In this study, we have proposed a novel spectral CT system design, Rainbow-CT, based on spectral modulation of poly-energetic X-ray source using balanced K-edge filter sets. We

have validated the system performance and estimated systematic errors by formulating a linear system equation in which a transmission matrix connects the measured filtered integrated intensity vector and energy-binned intensity vector. The energy-binned intensity vector was obtained by inverting this system equation, with the resultant independent set of energy-binned sinograms used to analytically generate energy-binned images. We have investigated the systematic errors for the Rainbow-CT method by assessing differences between simulation and experiment. Good agreement was found between the simulation and experimental results for most of materials and energy bins, holding out hopeful prospects for future model-based iterative image reconstruction efforts. The proposed spectral CT system design is feasible and could potentially provide a more accurate and cost-effective alternative to photon-counting spectral CT techniques, and is capable of operation at clinically relevant X-ray flux rates using currently available technology.

Acknowledgment

We would also like to thank Dr. Xing-qi Lu at Beth Israel Deaconess Medical Center for his help on the phantom study.

This work was supported in part by NIH grants R43-EB017591 and T32-EB013180.

References

1. Shikhaliev PM. The upper limits of the SNR in radiography and CT with polyenergetic x-rays. Phys Med Biol. 2010 Sep 21.55:5317–5339. [PubMed: 20736493]
2. Goodsitt MM, Christodoulou EG, Larson SC. Accuracies of the synthesized monochromatic CT numbers and effective atomic numbers obtained with a rapid kVp switching dual energy CT scanner. Med Phys. 2011 Apr.38:2222–2232. [PubMed: 21626956]
3. Meinel FG, Bischoff B, Zhang Q, Bamberg F, Reiser MF, Johnson TR. Metal artifact reduction by dual-energy computed tomography using energetic extrapolation: a systematically optimized protocol. Invest Radiol. 2012 Jul.47:406–414. [PubMed: 22659595]
4. Landry G, Reniers B, Granton PV, van Rooijen B, Beaulieu L, Wildberger JE, Verhaegen F. Extracting atomic numbers and electron densities from a dual source dual energy CT scanner: experiments and a simulation model. Radiother Oncol. 2011 Sep.100:375–379. [PubMed: 21924780]
5. Schlomka JP, Roessl E, Dorscheid R, Dill S, Martens G, Istel T, Baumer C, Herrmann C, Steadman R, Zeitler G, Livne A, Proksa R. Experimental feasibility of multi-energy photon-counting K-edge imaging in pre-clinical computed tomography. Phys Med Biol. 2008 Aug 7.53:4031–4047. [PubMed: 18612175]
6. Wang X, Meier D, Taguchi K, Wagenaar DJ, Patt BE, Frey EC. Material separation in x-ray CT with energy resolved photon-counting detectors. Med Phys. 2011 Mar.38:1534–1546. [PubMed: 21520865]
7. He P, Wei B, Cong W, Wang G. Optimization of K-edge imaging with spectral CT. Med Phys. 2012 Nov.39:6572–6579. [PubMed: 23127051]
8. Baturin P, Alivov Y, Molloi S. Spectral CT imaging of vulnerable plaque with two independent biomarkers. Phys Med Biol. 2012 Jul 7.57:4117–4138. [PubMed: 22683885]
9. Shikhaliev PM, Fritz SG. Photon counting spectral CT versus conventional CT: comparative evaluation for breast imaging application. Phys Med Biol. 2011 Apr 7.56:1905–1930. [PubMed: 21364268]
10. Taguchi K, Zhang M, Frey EC, Wang X, Iwanczyk JS, Nygard E, Hartsough NE, Tsui BM, Barber WC. Modeling the performance of a photon counting x-ray detector for CT: energy response and pulse pileup effects. Med Phys. 2011 Feb.38:1089–1102. [PubMed: 21452746]

11. Ding H, Molloi S. Image-based spectral distortion correction for photon-counting x-ray detectors. Med Phys. 2012 Apr.39:1864–1876. [PubMed: 22482608]
12. Carroll FE. Tunable monochromatic X rays: a new paradigm in medicine. AJR Am J Roentgenol. 2002 Sep.179:583–590. [PubMed: 12185024]
13. Crotty DJ, McKinley RL, Tornai MP. Experimental spectral measurements of heavy K-edge filtered beams for x-ray computed mammotomography. Phys Med Biol. 2007 Feb 7.52:603–616. [PubMed: 17228108]
14. Ross P. Polarisation of x-rays. Phys Rev. 1926; 28:425.
15. Boas F, Fleischmann D. CT artifacts: causes and reduction techniques. Imaging in Medicine. 2012; 4:229–240.
16. Lanier NE, Gerhardt SP, Den Hartog DJ. Low-cost, robust, filtered spectrometer for absolute intensity measurements in the soft x-ray region. Review of Scientific Instruments. 2001; 72:1188–1191.
17. Saito M. Quasimonochromatic x-ray computed tomography by the balanced filter method using a conventional x-ray source. Med Phys. 2004 Dec.31:3436–3443. [PubMed: 15651626]
18. Ducote JL, Alivov Y, Molloi S. Imaging of nanoparticles with dual-energy computed tomography. Phys Med Biol. 2011 Apr 7.56:2031–2044. [PubMed: 21386141]
19. Kirkpatrick P. On the Theory and Use of Ross Filters. Rev Sci Instrum. 1939; 10:186.
20. Hunemohr N, Krauss B, Tremmel C, Ackermann B, Jakel O, Greilich S. Experimental verification of ion stopping power prediction from dual energy CT data in tissue surrogates. Phys Med Biol. 2014 Jan 6.59:83–96. [PubMed: 24334601]
21. Siewerdsen JH, Waese AM, Moseley DJ, Richard S, Jaffray DA. Spektr: a computational tool for x-ray spectral analysis and imaging system optimization. Med Phys. 2004 Nov.31:3057–3067. [PubMed: 15587659]
22. Hsieh, J. Computed tomography: principles, design, artifacts, and recent advances: SPIE. Bellingham, WA: 2009.
23. Xia D, Roeske JC, Yu L, Pelizzari CA, Mundt AJ, Pan X. A hybrid approach to reducing computed tomography metal artifacts in intracavitary brachytherapy. Brachytherapy. 2005; 4:18–23. [PubMed: 15737902]
24. Berger, MJ.; Hubbell, JH.; Seltzer, SM.; Chang, J.; Coursey, JS.; Sukumar, R.; Zucher, DS.; Olsen, K. XCOM: Photon Cross Sections Database [Online]. Available: http://www.nist.gov/pml/data/xcom/
25. Richards A, D'Souza S. A novel NIR camera with extended dynamic range. SPIE Thermosence XXVIII. 2006:62050G-1–62050G-13.

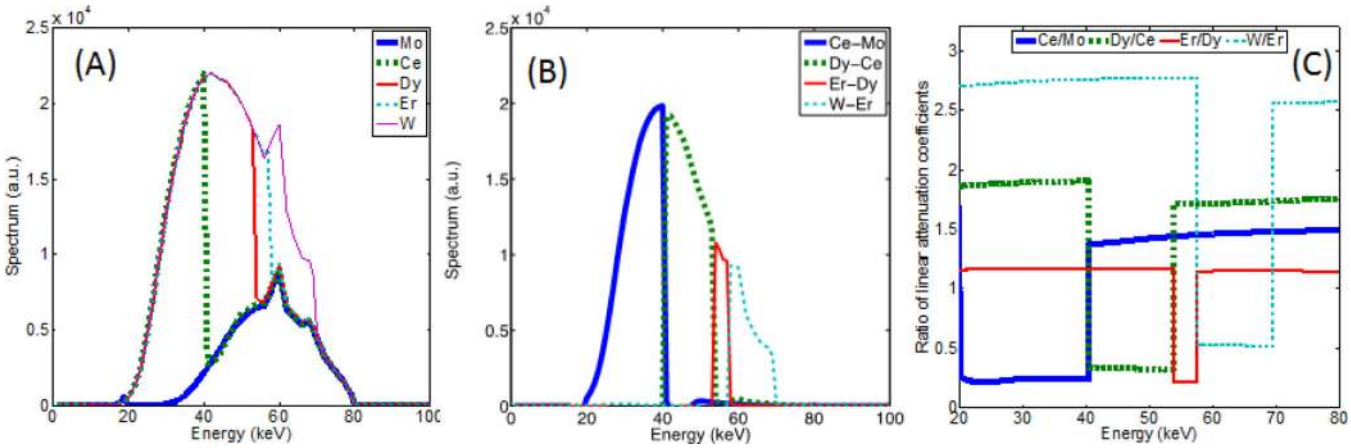

Fig. 1.

The principle of balanced K-edge filter set. (A) Filtered X-ray spectra; (B) Difference of consecutive spectra; (C) Ratio of linear attenuation coefficients of two consecutive filters.

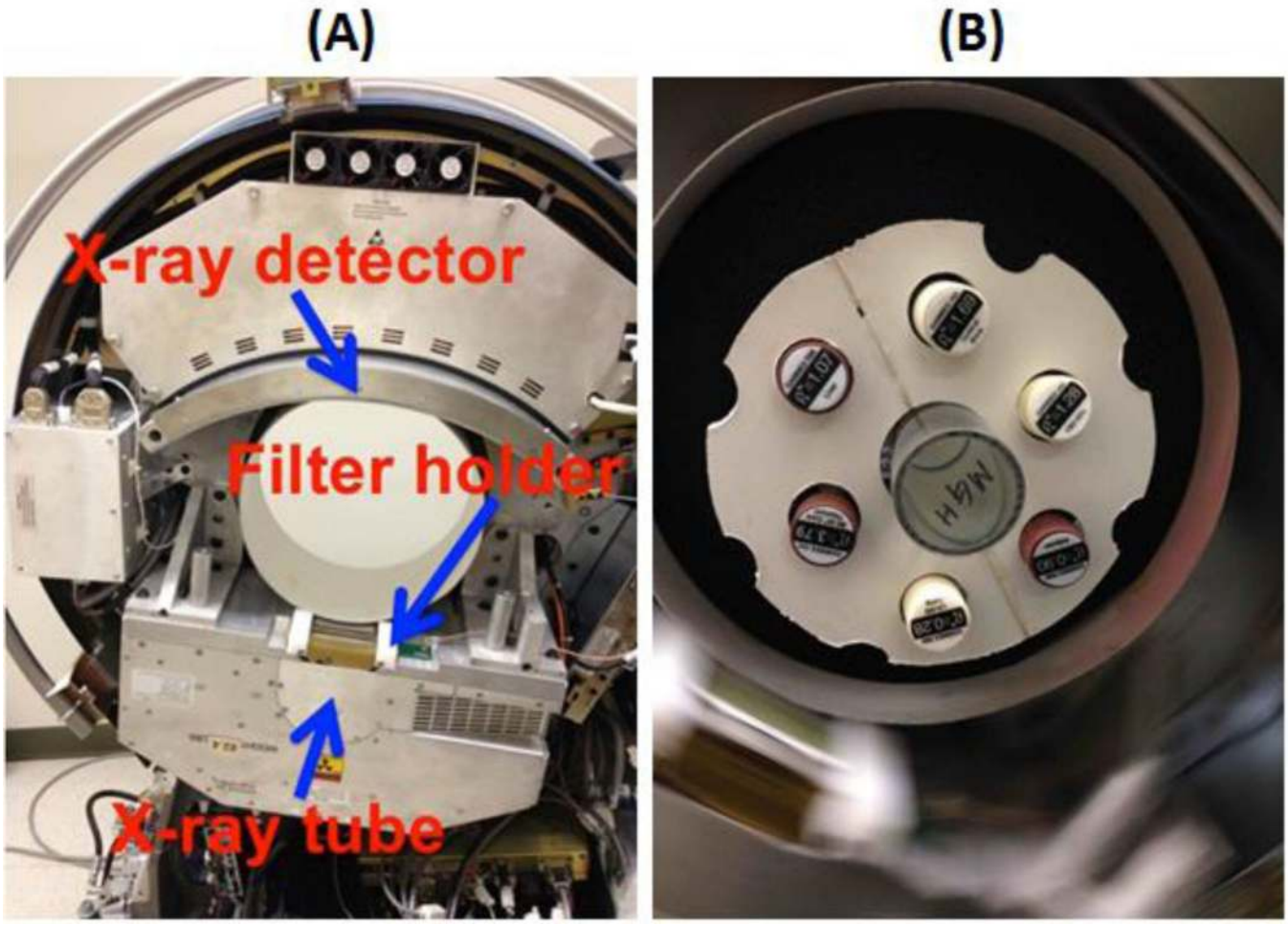

Fig. 2.
The CT scanner (A) and phantom (B) used for the experiment.

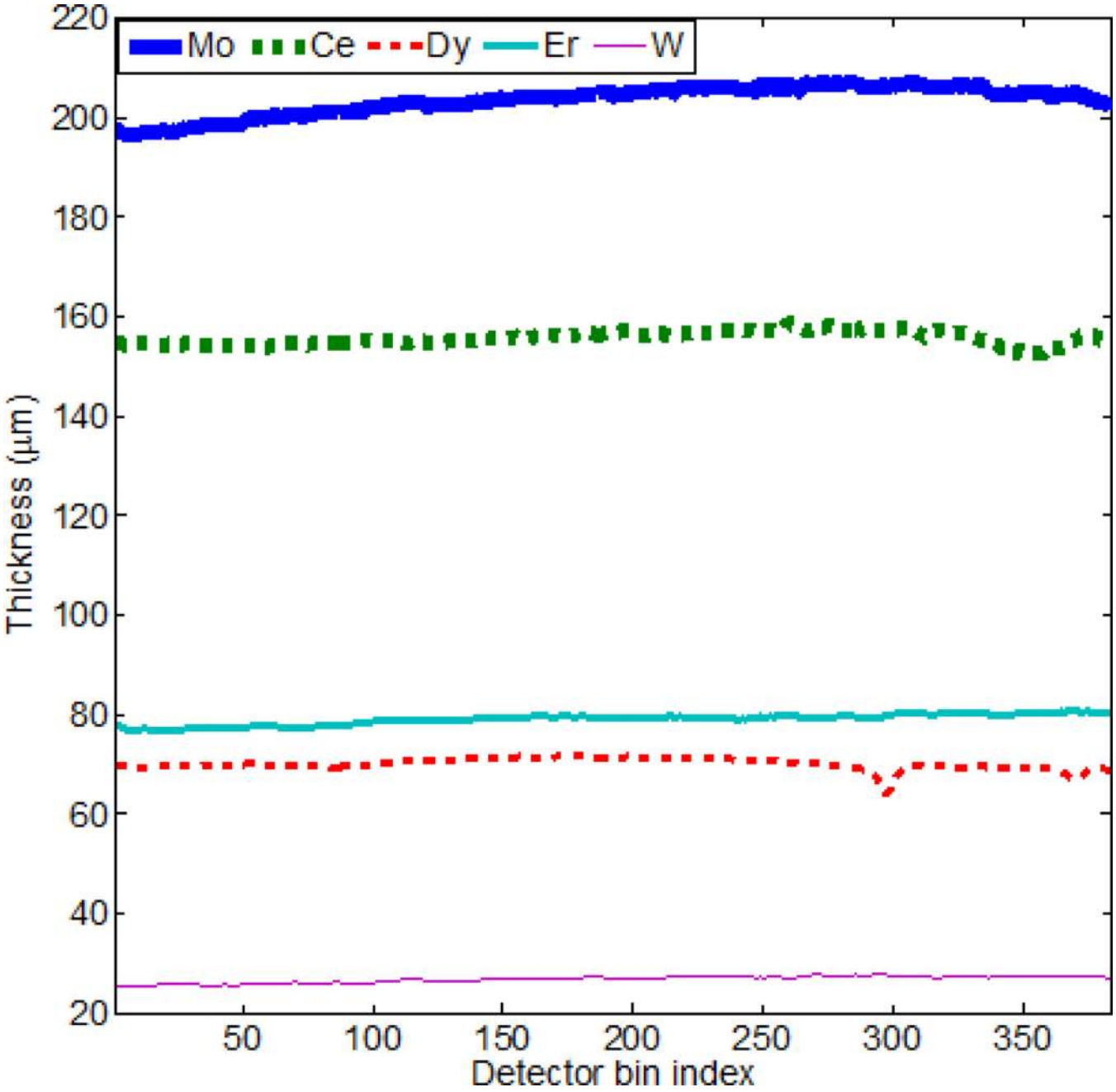

Fig. 3.
Measured interception thickness versus detector bin index for each filter used.

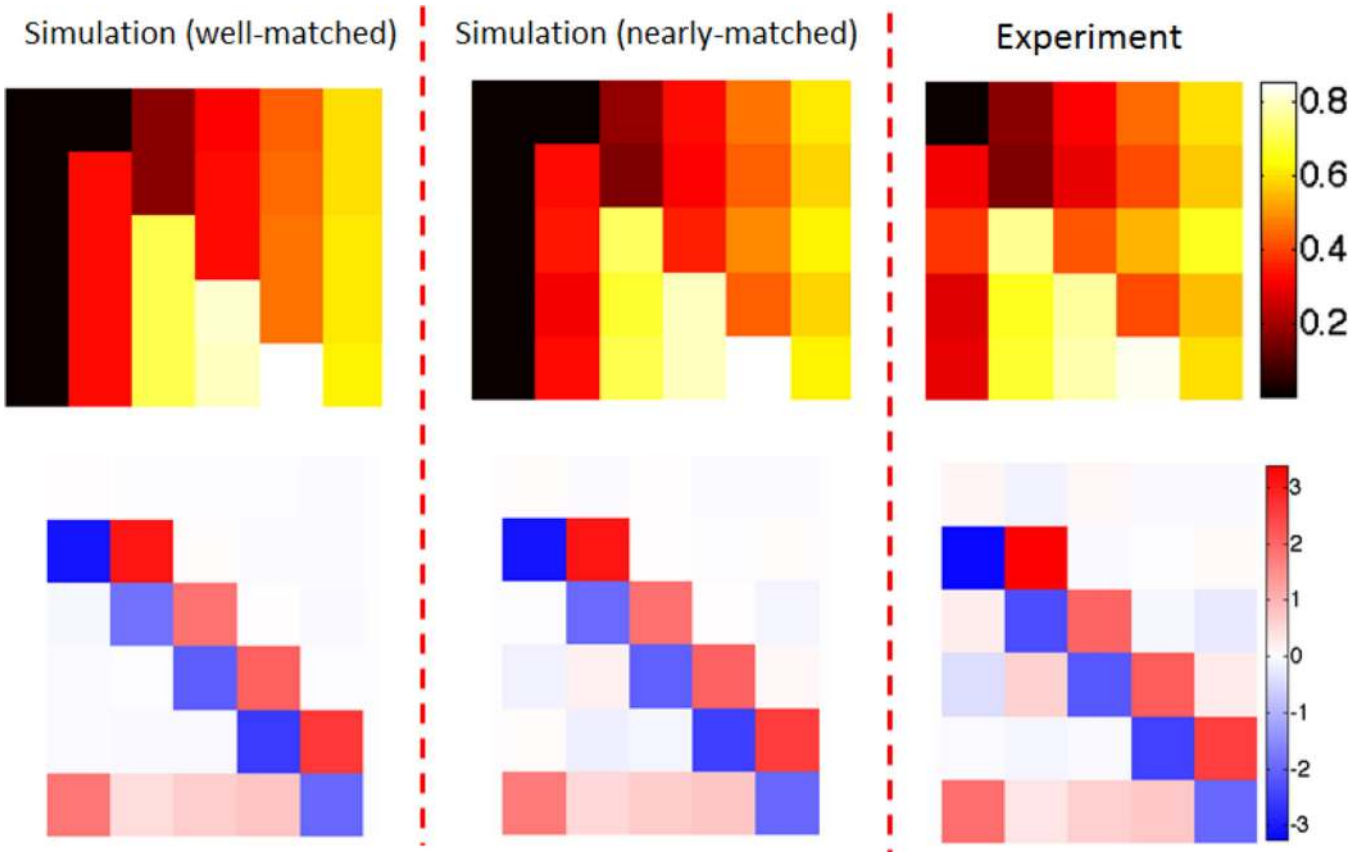

Fig. 4.

Transmission (top row) and its corresponding pseudoinverse (bottom row) matrices for one of the detector bins in the middle of the X-ray detector.

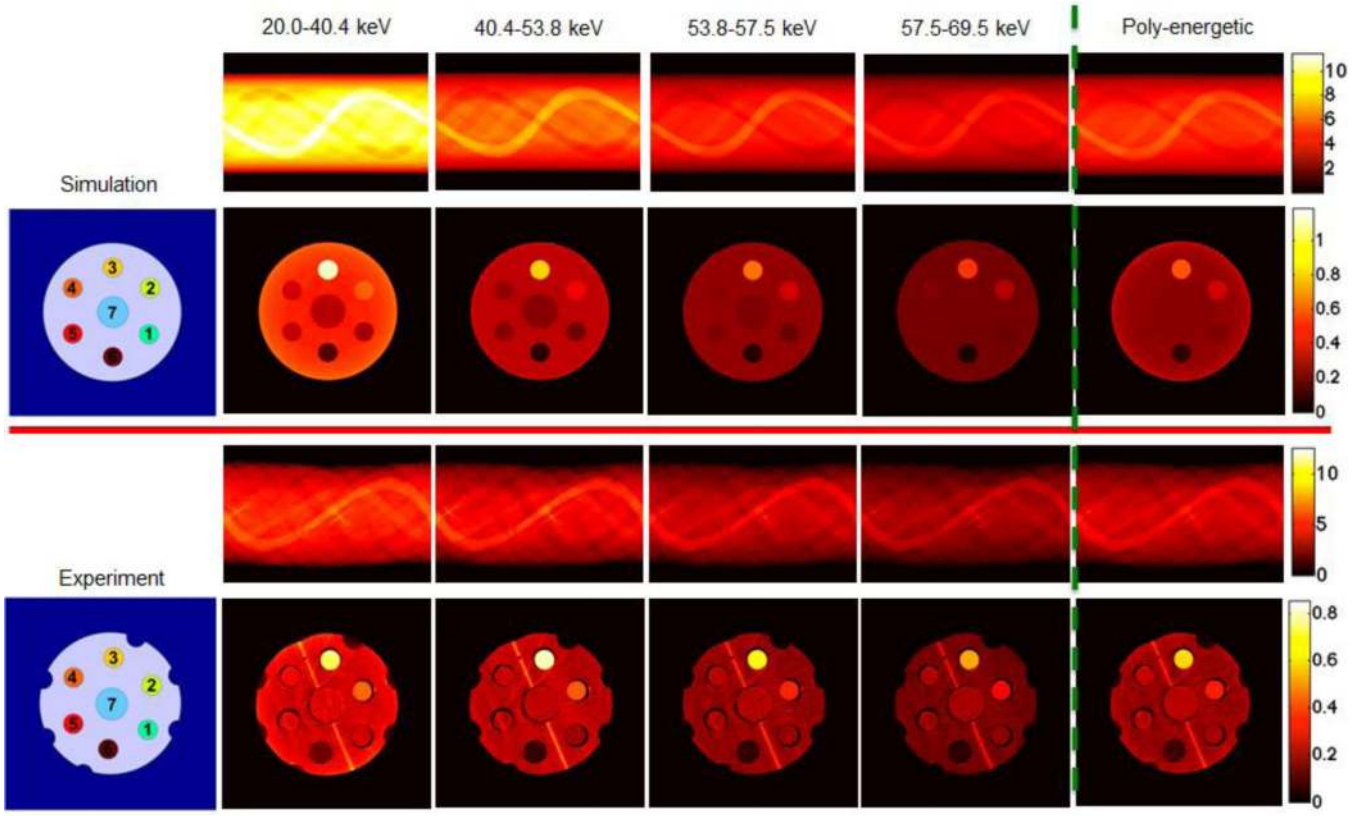

Fig. 5.

Energy-binned and poly-energetic sinograms and reconstructed μ images (cm^{-1}). The left side column shows the phantoms used in the simulation and experiment. Rods 1–7 are: 1) Adipose, 2) CB2-30, 3) Cortical Bone, 4) Liver, 5) Solid Water (Simulation)/Titanium Embedded Solid Water (Experiment), 6) Lung-300, and 7) Water, respectively. The bright diagonal line through the center of the experimental phantom is due to the glue used to attach the two semi-circular PVC pieces together [See Fig. 2(B)].

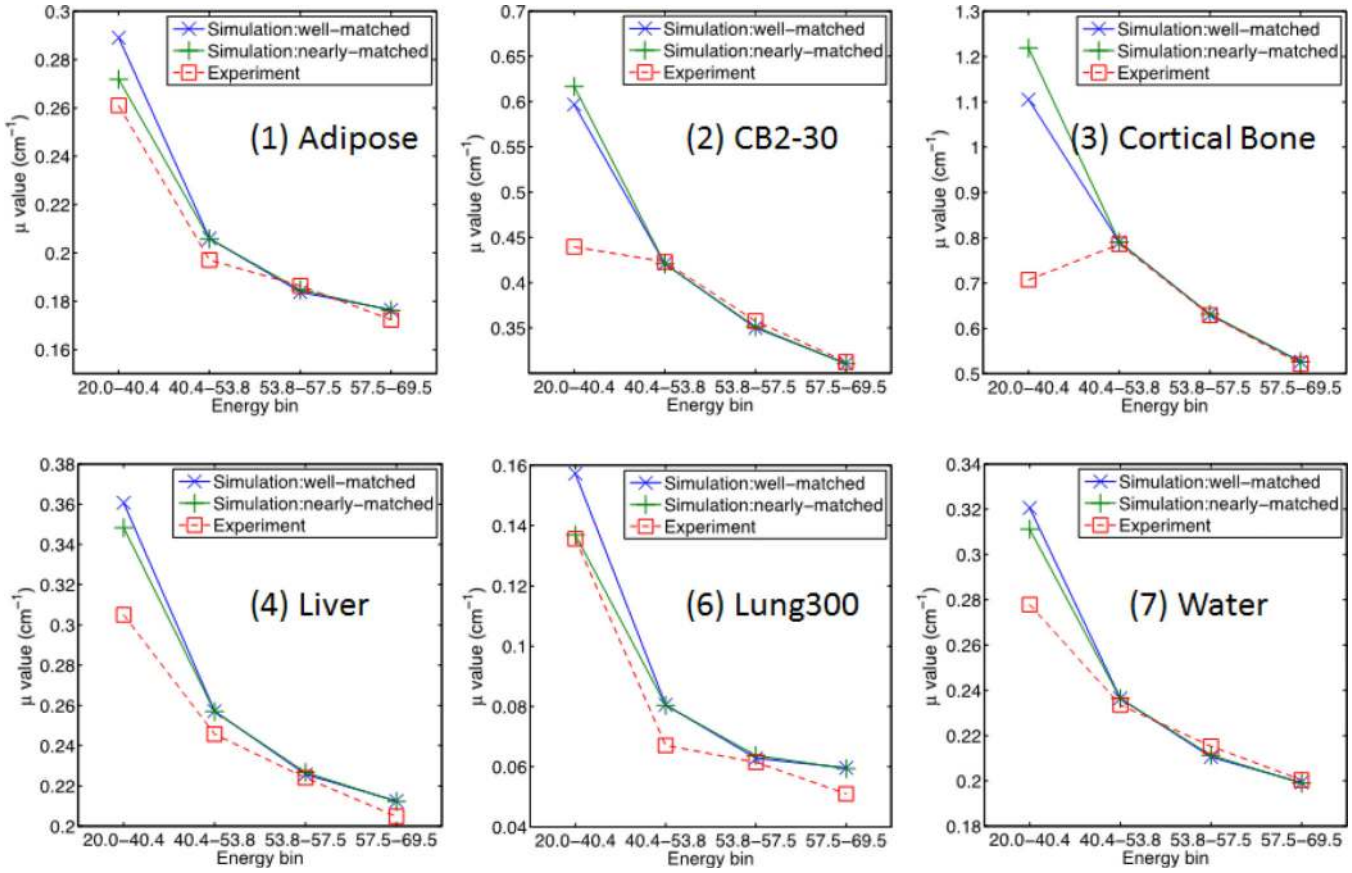

Fig. 6.

The ROI-averaged μ (cm^{-1}) versus energy bin for different materials.

TABLE I

Difference (in percentage) of ROI-averaged μ relative to the weighted average NIST value in the four energy bins.

	Simulation (well-matched) / Simulation (nearly-matched) / Experiment			
ROI	**20.0–40.4 keV**	**40.4–53.8 keV**	**53.8–57.5 keV**	**57.5–69.5 keV**
1. Adipose	10.5/3.9/3.1	3.1/3.0/−1.2	−1.0/−0.5/0.4	−1.0/−1.1/−3.3
2. CB2-30	−35.5/−33.3/−48.7	−6.0/−6.0/−5.0	−2.3/−2.0/0.0	−2.2/−2.3/−1.6
3. Cortical Bone	−49.7/−44.5/−64.7	−11.0/−11.0/−10.8	−3.0/−2.7/−2.7	−3.0/−3.1/−3.9
4. Liver	−7.8/−11.0/−18.1	0.2/0.1/−3.9	−1.5/−1.1/−2.1	−1.4/−1.5/−4.9
6. Lung-300	53.2/33.4/38.8	18.6/18.4/−0.9	3.3/4.7/1.1	4.0/3.5/−11.0
7. Water	−9.8/−12.4/−17.9	−0.6/−0.7/−1.6	−1.6/−1.2/0.7	−1.4/−1.5/−0.8